10th International Conference on Fracture Mechanics of Concrete and Concrete Structures
FraMCoS-X
G. Pijaudier-Cabot, P. Grassl and C. La Borderie (Eds)

MECHANICAL EVALUATION OF 3D PRINTABLE NANO-SILICA INCORPORATED FIBRE-REINFORCED LIGHTWEIGHT FOAM CONCRETE

SEUNG CHO[*], JACQUES KRUGER[†], STEPHAN ZERANKA[†], ALGURNON S. VAN ROOYEN[†] AND GIDEON P.A.G. VAN ZIJL [†]

Stellenbosch University
Stellenbosch, South Africa
e-mail: [*] scho@sun.ac.za
† pjkruger@sun.ac.za
szeranka@sun.ac.za
asvr@sun.ac.za
gvanzijl@sun.ac.za

Keywords: Mechanical Evaluation, Microstructure, Foam Concrete, Nanoparticles, Fiber Reinforced Concrete, 3D Printing

Abstract: Lightweight foam concrete (LWFC) is becoming an interesting structural material. In its fresh state, LWFC is highly flowable. Modification of the rheology is required to include 3D construction printing as a production process for this class of materials. Nanoparticles have been shown to improve thixotropy of cement-based materials, characterized by a high static yield shear stress, but a distinctly lower dynamic yield shear stress. In this paper, 2% nano-silica (n-SiO2) by mass of cement content is added to LWFC, and the consequential improved 3D printability validated by actual 3D printing of laboratory specimens. A systematic experimental study is performed to characterize the mechanical strength and stiffness, as well as fracture energy of n-SiO2 LWFC, against control LWFC without n-SiO2. The n-SiO2 specimens are prepared by both casting and 3D printing, in order to also investigate the influence of the layered 3D printing process, including the cohesion of the interfaces between layers. The mechanical strength, stiffness and fracture energy of n-SiO2 LWFC are shown to be significantly higher than control LWFC specimens without nanoparticles.

1 INTRODUCTION

Lightweight foam concrete (LWFC) originates from early in the previous century. Recent advances in LWFC strength have led to the possibility of its structural application [1, 2]. LWFC can be produced in a wide density range, and the range 1200 to 1600 kg/m^3 is believed to be most applicable for structural use. Improved bond between steel reinforcement bars and LWFC was required [3], and achieved in the development of a precast structural load-bearing wall system from reinforced LWFC (R/LWFC) by Dunn et al. [4].

To extend applications to free-form façade structural elements, 3D printing (3DP) of LWFC is developed by the authors. The composite comprises of cement, and other binders, fine aggregate and water as base mix, subsequently mixed with pre-formed foam. The combination is highly flowable, which complicates 3DP of LWFC, as it has too low static shear strength for shape retention of the 3D printed filament, or to support subsequent layers in the additive manufacturing process. Based on the potential of nanomaterials to enhance fresh and hardened properties of cement-based composites [5], Kruger et al. [6]

developed a highly thixotropic 3D printable mortar using low volumes of nano-Silica (n-S). This contribution presents the influence of n-S on the hardened properties of LWFC.

2 EXPERIMENTAL PROCEDURES

2.1 Material mix design

The conventional highly flowable LWFC [3, 4] is modified for 3D printing. The appropriate degree of thixotropy is primarily attained by the addition of nano-Silica (n-SiO_2) particles, which have large specific surface area, (150±30 m^2/g). A n-SiO_2 dosage of 2% of the cement mass is used. In addition, water content is reduced to increase the fresh-state static yield stress. Low water content matrix forms drier base mix which may reduce the stability of the foam in the matrix because the hydration may absorb the moisture on the surface of the foam. Small cone slump flow diameter measurements according to ASTM C230/C230M [7] were reduced to be in the range 180 to 200 mm, while 220 to 250 mm has been reported to be appropriate for conventional LWFC [1]. The impact of the lower flow range indeed yield a larger variation from the wet target density of 1400 kg/m^3 used in this research project (see Section 3 for the results). However, the matrix displayed noticeable enhancement in degree of thixotropic performance, which greatly improves 3D printability. Table 1 gives the mix composition.

Four sets of specimens were prepared and tested. The first set is the Control set, and contains no fibre or n-SiO_2. The second set is denoted PP, and contains 0.45% (by volume) Polypropylene (PP) fibre (length 6 mm, diameter 40 μm), but no n-SiO_2. The third set, nSPP, contains 0.45% PP fibre as well as 2% (of cement mass) n-SiO_2. Specimens from these three sets were prepared by standard casting in moulds for characterisation testing.

A fourth set, denoted nSPP(3D) has the same mix design as nSPP, but was 3D printed, in order to study the influence of the printing process, as well as interfaces in 3D printed specimens. Table 2 summarises the four test sets. A gantry-type 3D concrete printer built by the authors was used for the 3D printing, which produced a layer height in the range of 12-15 mm, with a circular printer nozzle diameter of 25 mm, set at a speed of 40 mm/s.

Table 1: Mix design of LWFC

Constituents	Type	RD	Mass (kg/m^3)
Cement	CEM II 52.5N	3.15	498.1
Fly-ash	Class S	2.20	498.1
Sand	Silica fine sand	2.65	99.6
Water		1.0	281.9
Fibres	Polypropylene	0.91	4.10
Foam		0.075	22.2
Nano SiO_2 (n-SiO_2)	20-30 nm particle size (99.5% purity)	0.20	9.96

Table 2: Test set configuration

	Control	PP	nSPP	nSPP(3D)
No.	1	2	3	4
Fibre	X	✓	✓	✓
n-SiO_2	X	X	✓	✓

2.2 Mechanical evaluation

In this study, fracture energy, compression strength, and Young's modulus are assessed for the mechanical performance evaluation of LWFC.

For fracture energy determination, the JCI notched beam test for conventional and fibre-reinforced concrete respectively [8, 9] is used. As the mix is comprised of fine particles only, the beam size is set to be 40x40x160 (BxDxL) mm. A 12 mm deep notch, which complies with the 0.3D requirement, is sawn at the centre of the span. The beam specimens are either cast in steel moulds of the correct size (Control, PP, and nSPP), or 3D printed (nSPP(3D)) and saw-cut into size. Three point loading is performed on the beams, controlled by the crack mouth opening displacement (CMOD) rate, set at 0.04 mm/min in an Instron Materials Testing Machine (MTM). The load-CMOD response is recorded and used for the determination of the fracture energy (G_f) in N/m. The flexural strength (σ_{flex}) of the material is determined from the elastic formulation as follows:

$$\sigma_{flex}=3FL/(2BD^2) \quad (1)$$

Due to insufficient strength development for central notch cutting at an early age (7 days) in some of the sets, the test is only carried out at the ages of 14 and 28 days.

After the three-point bending test, the undamaged ends of the 40x40x160 mm beams are used for the determination of compression strength (EN 196-1 [10]). For the compression test, the sample is placed between two 40x40x10 mm steel platens in the MTM.

In the case of the 3D printed beam, 40 mm cubes are saw-cut from the beam specimens after the flexural test. Two orientations are cut, as illustrated in Fig. 1, which enable compression testing perpendicular to the layer interfaces (Direction 1), and a second set tested parallel to the layer interfaces (Direction 2).

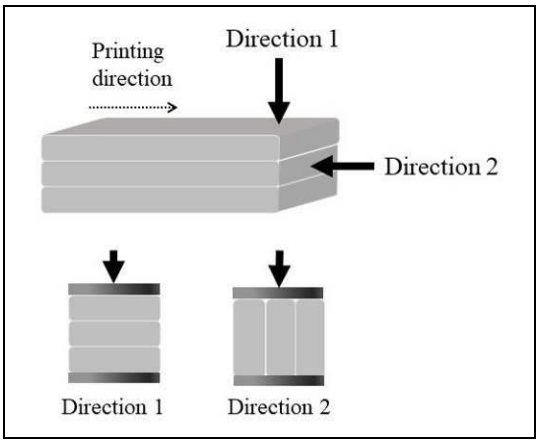

Figure 1: 3D printed LWFC specimen preparation.

Cylindrical specimens 100 mm in diameter and 200 mm high are prepared for Young's modulus tests according to ASTM C469-02 [11]. The specimen is loaded up to 40% of compressive capacity. Displacement under this load is taken as the average reading of three LVDTs, spaced at 120° around the specimen circumference, over a 70 mm gauge length along the cylinder central height. Three specimens are used per test set.

All specimens were stored in a climate-controlled room at 23±2°C and 65±5% RH during the entire curing period after stripping, or saw-cutting. Moreover, the densities are recorded before the test at each age.

2.3 Interlayer bond strength

Unlike conventionally cast specimens, the 3D printed specimens are produced by layer deposition, which may result in non-homogeneity between the printed layers. The bonding material parameter, interlayer bond strength (IBS), has become an important material design parameter for 3D printing. For the IBS measurements, several test methods have been proposed such as a direct tensile test [12], and indirect tensile testing in flexure [13] for the mode I behaviour. For mode II, a shear test has been proposed [14].

In this paper, the triplet shear test for brick and mortar joints, EN 1052-3 [15], is performed without lateral confinement, to measure the shear strength within the interface of the printed specimens. Figure 2 shows a schematic of the test setup. The peak shear strength f_{voi} is calculated as follows:

$$f_{voi}=F_{i,max}/(2A_i) \quad (2)$$

where $F_{i,max}$ is the ultimate load and A_i is the shear plane area of each interface.

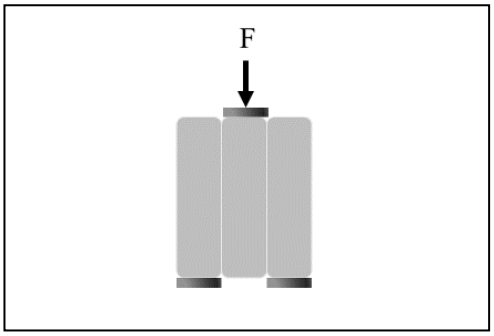

Figure 2: Triplet shear test setup illustration

2.4 Microstructure evaluation

The microstructure is analysed by scanning electron microscopy (SEM) in a Zeiss MERLIN SEM apparatus at the Central Analytical Facility of Stellenbosch University. This investigation is ongoing, but pore dispersion and size distributions are compared for the different test sets by visual observation on SEM images. The morphological differences can be captured, which may be anticipated by the nanoparticle incorporation.

3 EXPERIMENTAL RESULTS

3.1 Mechanical evaluation

The mechanical performance of LWFC is highly dependent on the density. The recorded densities are presented in Fig.3. The higher density from the test set nSPP is acquired due to the high stiffness of the base mix in the fresh state. Note that, despite the stiff nature of this mix, the spreadability matched the set criteria (180 – 200 mm) of the flow table diameter measurement under agitation caused by the impact of the flow table device. This correlates with high static yield stress, but lower dynamic yield shear stress which enables 3D printing. However, the high static stiffness may hinder the placement of the surfactant. Although the weight gain is considered to be inevitable, its mitigation in balancing appropriate thixotropy and light weight should be managed in future research.

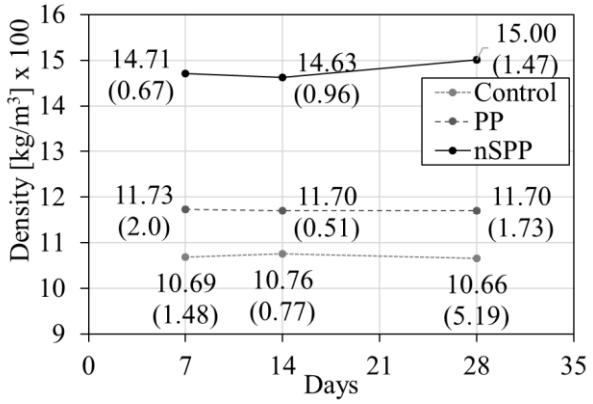

Figure 3: Density measurements (Coefficient of variation is expressed as % in brackets)

The complete set of mechanical test results are summarised in Table 3. Significant increase in fracture energy, flexural strength, compressive strength and E-modulus is observed at all test ages for the mix containing n-SiO_2. Averaged load-CMOD responses at 14 and 28 day ages are presented in Fig. 4, clearly showing the significantly enhanced strength and fracture energy by n-SiO_2 inclusion. Note that poor calibration of the clip gauge led to uncontrolled post-peak response of the nFSi specimen at the age of 28 days, which is also clear from the response for this test set in Fig. 4b.

Table 3: Mechanical test results (coefficient of variation is given in brackets as %)

	Day	Control	PP	nSPP	nSPP(3D)
Fracture energy, G_f [N/m]	14	7.04 (13.8)	14.18 (5.9)	17.52 (5.5)	24.17 (10.8)
	28	8.36 (18.4)	10.21 (28.6)	12.61* (38.7)	24.46 (15.1)
Flexural strength, $f_{flexure}$ [MPa]	14	1.38 (6.7)	1.49 (27.5)	2.70 (6.4)	2.33 (7.9)
	28	1.11 (11.0)	1.38 (27.3)	3.78 (7.9)	2.43 (13.1)
Compression strength, f_{cu} [MPa]	7	3.99 (16.2)	4.92 (5.2)	24.51 (2.8)	
	14	7.74 (9.0)	10.64 (6.7)	27.62 (8.1)	
	28	8.19 (5.3)	11.62 (10.1)	31.12 (4.6)	
Young's modulus, E [GPa]	7	6.77 (10.3)	7.56 (7.9)	13.65 (10.7)	
	14	6.46 (3.9)	7.29 (4.2)	12.26 (10.2)	
	28	6.41 (0.9)	7.09 (5.5)	13.78 (1.4)	

*Partial data. After the peak, some data was lost due to the poor clip gauge calibration.

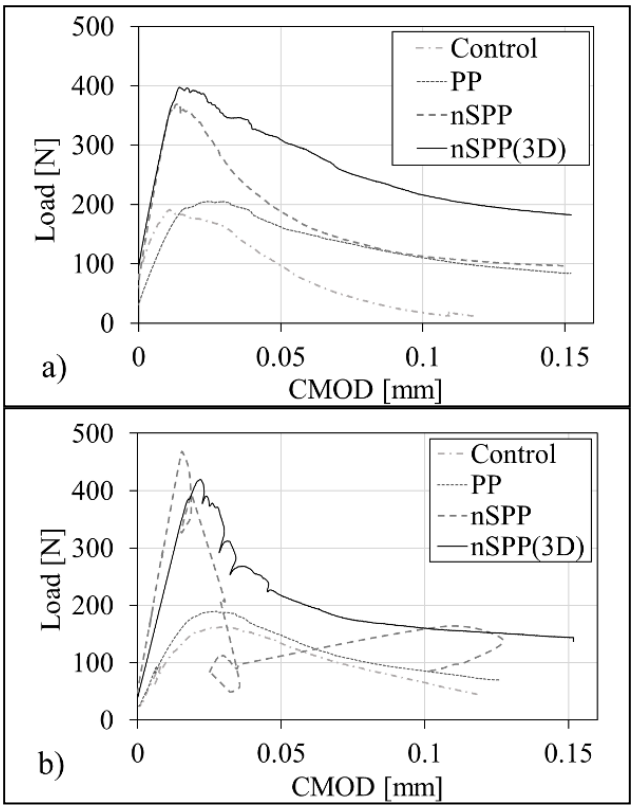

Figure 4: a) 14 days load-CMOD curve; b) 28 days load-CMOD curve. Note that the result of 28 days nSPP is due to the poor clip gauge calibration.

The compression test results and photos of the nSPP(3D), i.e. 3D printed specimens tested in two orthogonal directions, are summarised in Table 4. Figure 5 presents the compressive force against the cross-head displacement for these tests in a Zwick Z250 MTM. The peak strengths are lower than those of the cast specimen of the same mix (nSPP), reaching 50.7% and 67.0% of the average 28 day strength of cast specimens (nSPP) in Direction 1 and 2 respectively. It was also observed that no interfacial shear failure between the printed layers by fracture mode 1 and 2 which is related to IBS had not been found before the material matrix failure. While compressive splitting cracks are observed in both specimen test orientations in Table 4, it was thought that alignment of weak interfaces with the splitting cracks in Direction 2 would lead to lower compressive strengths. However, this was not the case. It appears that the interfaces have high strength, causing splitting cracks away from the interface region (Direction 2, Table 4). Also, it is likely that higher compressive strength arises in the composite in the printing direction. This remains to be confirmed in further research.

The Direction 2 load-displacement curve displays a few local peaks in the ascending load-deformation branch, ascribed to splitting crack formation before the ultimate peak is reached.

Table 4: Two directional, 28 day compression strength test results. Coefficient of variation given in brackets.

Direction	f_{cu} [MPa]	
1 Perpendicular	15.79 (3.2)	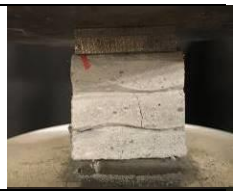
2 Longitudinal	20.85 (9.9)	

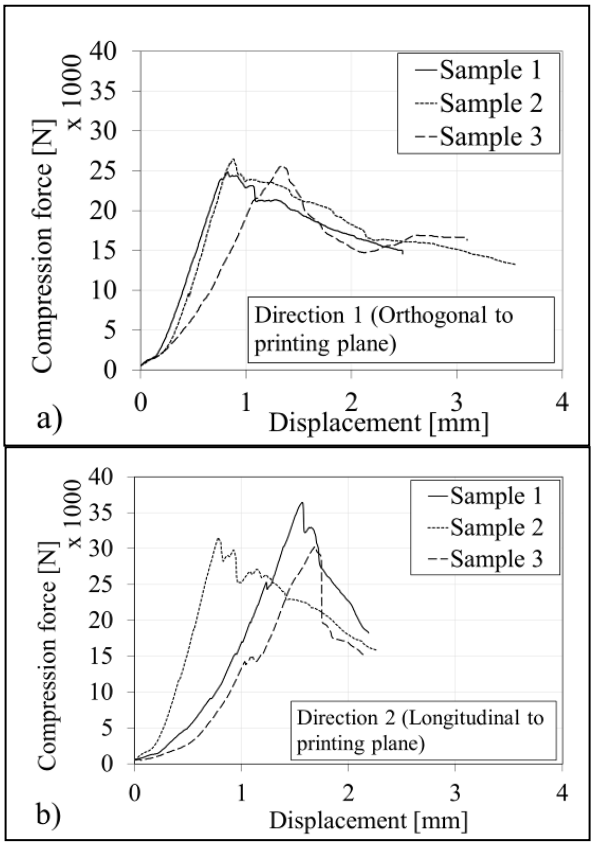

Figure 5: Compression load-displacement response of a) Direction 1 (perpendicular to the printing plane); b) Direction 2 (longitudinal to the printing plane).

In all aspects, the test results clearly show that nanoparticle addition considerably enhances the mechanical performance of LWFC, although it must be noted that a higher density was recorded for the test sets containing n-SiO_2. Two further, notable time-dependent observations are:

- The rate of compression strength development in the first 7 days is significantly lower in test sets without n-SiO_2 than in those with n-SiO_2. However, between 7 and 28 days, the strength gain rate slows down for the specimens with n-SiO_2.
- Young's modulus shows a slight reduction over time for all test sets, from 7 to 28 days.

3.2 Interlayer bond strength

Triplet tests are performed on three 40 mm cube specimens sawn from 3D printed LWFC beam specimens (nSPP(3D)). A failure mechanism of combined mode I and II fracture

is observed. Figure 6 shows the failure shapes and measured peak stress (f_{voi}) where 1.90MPa average stress and 22% coefficient of variation for the samples are acquired. Sample 1 delaminated along the interface and resulted in the largest shear strength, which can be considered representative of the interfacial cohesion. In sample 2, failure occurred within the printed layer. Sample 3 showed the combination of the failure mechanisms of sample 1 and 2. It was observed that the right vertical interfacial crack commenced first.

3.3 Microstructure evaluation

A roughly 10x10 mm fragment was obtained from each set from the failure surface of the three-point bending test, oven dried to completely remove the moisture in the matrix and subsequently used in SEM investigation. In Fig. 7 average pore size and numbers are seen to reduce with inclusion of n-SiO_2 which can be correlated with the increase in density observed. The magnification factor was 80.0x for all images. Larger pores are observed in the control and PP mix where nSPP mainly has smaller pores (< 200 μm) and more even distribution is observed. The 3D printed specimen shows a flattened, elongated pore shape due to the pumping pressure during 3D printing.

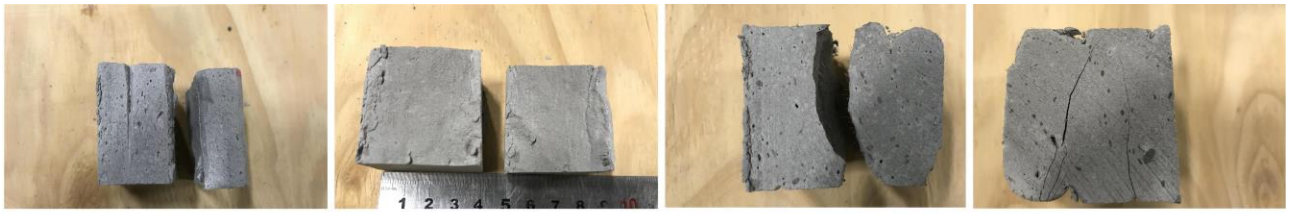

a) Sample 1: 2.29 MPa | b) Sample 1: delaminated surface | c) Sample 2: 1.61 MPa | d) Sample 3: 2.20 MPa

Figure 6: Triplet shear test specimens and result. The peak strengths, f_{voi}, are given in the figure.

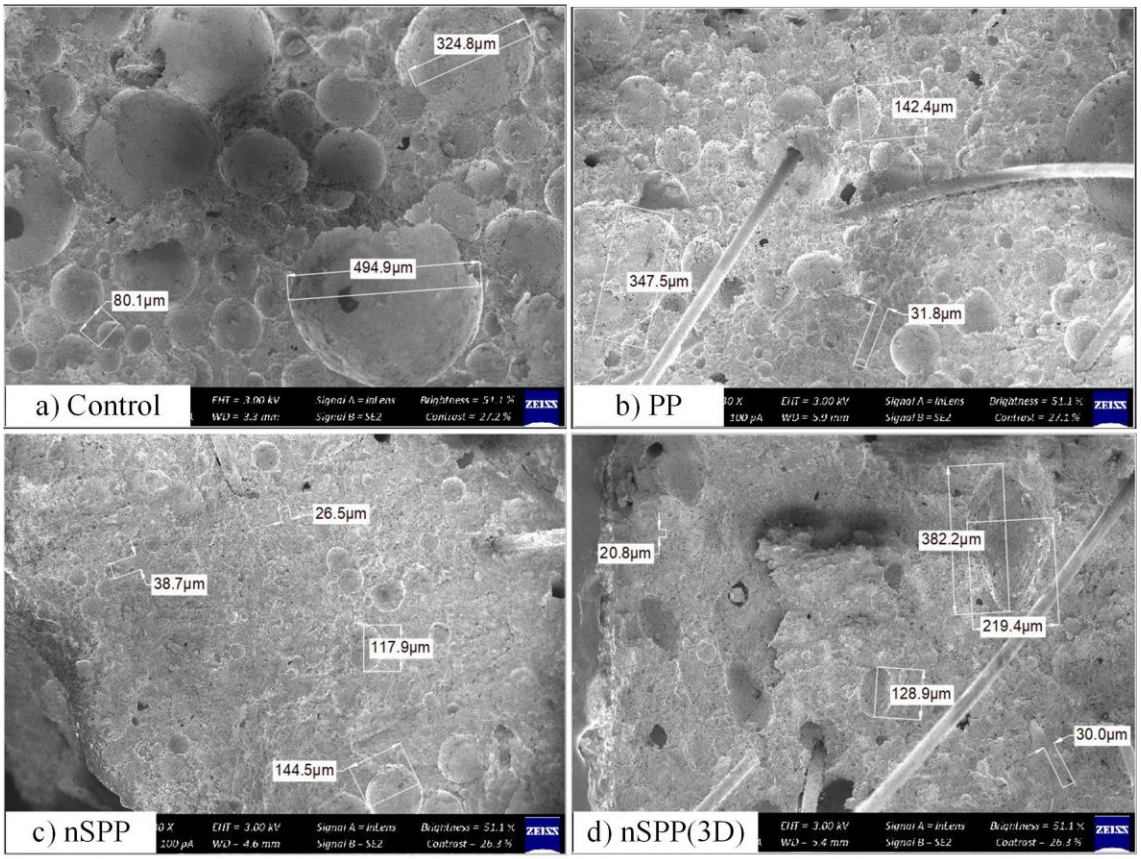

Figure 7: SEM photos (x80.0 magnification) of pore distribution and size for all test sets.

It appears from the images that the nanoparticles helped to form a dense matrix, ascribed to its high surface to volume ratio, and pozzolanic reaction [5]. The larger specific surface area of nanoparticles accelerates physical interaction towards improved dispersion, as well as chemical reactivity, which leads to formation of hydration products that fill the interstitial gaps between the particles and strengthens the matrix [5]. This is corroborated by the significantly enhanced mechanical strength and stiffness test results compared with normal LWFC.

Figure 8 illustrates morphological differences in the presence of nanoparticles. The nanoparticle incorporated matrix forms longer and larger amounts of needle or rod-like hydration products, which accommodate matrix bridging capacity and improved mechanical strength.

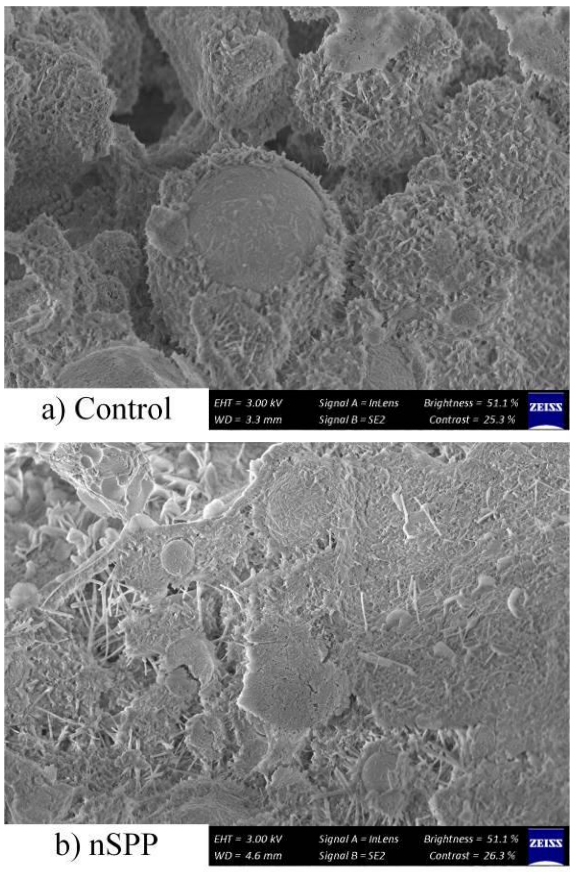

Figure 8: SEM photo (x5.0k) illustrating the morphological difference between the control and nanoparticle incorporated mix.

4 DISCUSSION

The nSPP mix has larger compression strength (Table 3). In addition, the early strength development, followed by a reduced strength development rate can be seen in Fig. 9. In the figure, the strengths are normalised by each test set's 28 day strength (f_{cu}) value.

While 40 to 50% of the 28 day strength is achieved at the age of 7 days in the control specimen sets without n-SiO_2, an average 7 day strength approaching 80% of the 28 day strength of the nSPP specimens is seen in Fig. 9. The high specific area of the nanoparticles contribute to the rate and amount of hydration product, particularly alite in the early stage [16]. It is thus worthwhile to investigate early stage strengths to verify the postulation.

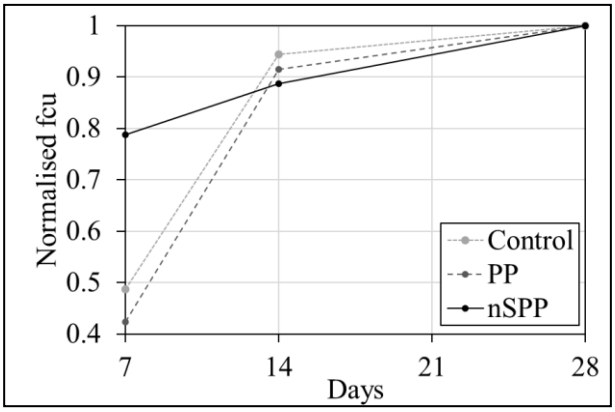

Figure 9: Normalised f_{cu} to 28 days strength

The elastic moduli are found to be inconclusive due to the diminishing trend with time, which conventionally develops with time. Note that the same samples were used throughout the testing period, i.e. the cylinders used for 7 day E-modulus tests, were returned to the climate controlled environment, and used for the E-modulus tests on 14 and 28 days. This might have led to micro-cracking in the specimens, whereby the E-modulus may be affected in subsequent tests on the same specimen.

5 CONCLUSION

Due to the potential of automated construction with lightweight foamed concrete, research into the mechanical

properties of 3D printable foam concrete has been investigated. The inclusion of small amounts of nano-silica enabled 3D printing of the foam concrete reported here, and characterisation testing became possible. The following conclusions are drawn:

- Nano-silica incorporation substantially improves the mechanical properties of foam concrete, in terms of compressive strength, elastic modulus and fracture energy, compared with a control mix.
- Microstructural assessment showed finer and more even pore structures in nano-silica incorporated LWFC. Morphological differences are present which confirm the enhanced mechanical performance.
- Interfacial cohesion between 3D printed layers introduced by the layered, additive manufacturing process was evaluated by means of a triplet shear test. Failure mechanisms included mode I and II fracture, whereby the interfacial bond is not clearly lower than the inherent shear strength of the 3D printed material.

REFERENCES

[1] Kearsley, E.P., Mostert, H.F., 2005. Designing mix composition of foamed concrete with high fly ash contents. *In: Proc., Int. Conf. on the Use of Foamed Concrete in Construction*. Thomas Telford, London, pp. 29–36.

[2] Jones, M.R., McCarthy, A., 2005. Preliminary views on the potential of foamed concrete as a structural material. *Magazine of Concrete Research* **57.1**: 21–31.

[3] de Villiers, J.P., van Zijl, G.P.A.G., van Rooyen, A.S., 2017. Bond of deformed steel reinforcement in lightweight foamed concrete (LWFC). *Structural Concrete*. **18(3)**:496-506.

[4] Dunn, T.P.A., van Zijl, G.P.A.G., van Rooyen, A.S., 2018. Investigating a reinforced lightweight foamed concrete walling system for low-rise residential buildings in moderate seismic regions. *Journal of Building Engineering*. **10**: 663-670.

[5] Paul, S.C., van Rooyen A.S., van Zijl, G.P.A.G., Petrik., L.F., 2018. A review of nanoparticles in cement-based materials. *Construction and Building Materials*. **189**: 1019-1034.

[6] Kruger, P.J., van Zijl, G.P.A.G., Cho, S., Zeranka, S., 2018. Multi-physics approach for improved thixotropy of cement-based materials for 3DPC. *Proceedings 3DCP*, 26-28 November 2018, Melbourne, Australia.

[7] ASTM C230/C230M, 2014. Standard specification for flow table for use in tests of hydraulic cement.

[8] JCI-S-001, 2003. Method of test for fracture energy of concrete by use of notched beam.

[9] JCI-S-002, 2003. Method of test for load-displacement curve of fiber reinforced concrete by use of notched beam.

[10] BS EN 196-1, 2005. Methods of testing cement. Determination of strength.

[11] ASTM C469 – 02, 2002. Standard Test Method for Static Modulus of Elasticity and Poisson's Ratio of Concrete in Compression.

[12] Sanjayan, J.G., Nematollahi, B., Xia, M., Marchment, T., 2018. Effect of surface moisture on inter-layer strength of 3D printed concrete. *Const. and Build. Mat.* **172**:468-75.

[13] Kruger, P.J., van den Heever, M., Cho., S., van Zijl, G.P.A.G., High-performance 3D printable concrete enhanced with nanomaterials. *Proceedings RILEM SMSS*, 18-22 March 2019, Rovinj, Croatia.

[14] Zareiyan, B. and Khoshnevis, B., 2017. Effects of interlocking on interlayer adhesion and strength of structures in 3D printing of concrete. *Automation in Construction*. **83**:212-21.

[15] EN 1052-3. 2007. *Methods of test for masonry. Part 3: Determination of initial shear strength*.

[16] Ye, Q., Zhang, Z., Kong, D., Chen, R., 2007. Influence of nano-SiO2 addition on properties of hardened cement paste as compared with silica fume. *Construction and Building Materials*. **21(3)**:539-545.